# Impact of Hydrothermal Processing Conditions on High Aspect Ratio Titanate Nanostructures

Robert Menzel, Ana M. Peiró, James R. Durrant, and Milo S. P. Shaffer*

*Department of Chemistry, Imperial College London, South Kensington Campus, SW7 2AZ, London, United Kingdom*

*Received July 24, 2006. Revised Manuscript Received September 19, 2006*

High aspect ratio $TiO_x$ nanostructures were produced by simple hydrothermal treatment and the nature of two distinct morphologies, compact nanofibers and hollow nanotubes, was explored as a function of preparation conditions. The crystal phase of the $TiO_2$ starting material was found to be a key parameter for the determination of the general morphology, whereas particle size mainly influenced the conversion yield. Other parameters, such as hydrothermal temperature and solid/liquid ratio, exert control over the size and shape of the product. The findings can be interpreted in terms of a dissolution/recrystallization formation mechanism. Detailed characterization by Raman spectroscopy and X-ray/electron diffraction is provided; the data show that the nanoscale products were based on a variety of hydrated and often sodium-containing titanate crystal phases, such as trititanate or pentatitanate, rather than anatase or rutile. Variations in the washing procedure were found to have no significant influence on the overall morphology of the products, but did affect other properties, such as the specific surface area and annealing behavior, that are important for many practical applications.

## Introduction

There has been widespread recent interest in high aspect ratio nanostructures, and particularly nanotubes, from titania precursors. These structures combine high aspect ratio, high surface area, and versatile chemistry with the conventional advantages and properties of $TiO_2$. They are thought to have potential benefits in a wide range of applications, including catalysis,[1] energy storage,[2] gas sensors,[3] and photovoltaics.[4] Our research is motivated by the need to produce improved, nanostructured $TiO_x$ materials for use as semiconducting electrodes in hybrid organic−inorganic and dye-sensitized solar cells (DSSCs).[5] Titania structures with high aspect ratios are expected to facilitate electron transport[6] and may enhance dye adsorption and interpenetration of hole transport materials,[4] all important factors in the cell performance. For this application, the relationship between the synthesis conditions and the morphology of the resulting titania must be understood, especially including the effects on critical properties such as crystal phase, specific surface area, and annealing behavior.[7]

One of the most promising and simplest synthetic routes to high aspect ratio $TiO_x$ nanostructures is the hydrothermal treatment of titania powders in highly basic solution at moderate temperatures, pioneered by Kasuga.[8] It has often been claimed that this process yields single-crystal nanotubes with a uniform outer diameter of around 10 nm and a length of several hundreds nanometers.[2,9,10] More recently, other morphologies such as nanofibers and nanoribbons have also been reported using related hydrothermal treatments.[11,12] However, statements in the literature concerning the impact of the various preparation conditions on the resulting structures are often conflicting and inconsistent. Hydrothermal parameters such as reaction temperature, solid−liquid ratio, and reaction time differ over a broad range, and different morphologies are reported for very similar synthetic conditions. For instance, Tsai et al.[13] found that for temperatures higher than 130 °C, additional granular particles are formed; Yuan et al.[11] reported that the optimum yield of nanotube formation is achieved at 150 °C, whereas the formation of high aspect ratio nanoribbons is observed only at temperatures higher than 180 °C. Moreover, some authors argue that the formation of the nanostructures occurs during the final washing step, in which the base used during the hydrothermal treatment is neutralized. They demonstrate that the washing conditions crucially determine the size and shape of the formed structures.[8,10] However, other groups report that the desired structures are already present during the basic hydrothermal treatment, before neutralization.[14,15]

* Corresponding author. E-mail: m.shaffer@imperial.ac.uk.

(1) Zhu, H. *J. Am. Chem. Soc.* **2005**, *127*, 6730.
(2) Zhang, S.; Peng, L.-M.; Chen, Q.; Du, G. H.; Dawson, G.; Zhou, W. Z. *Phys. Rev. Lett.* **2003**, *91*, 256103.
(3) Zhu, Y. *Anal. Chem.* **2002**, *74*, 120.
(4) Adachi, M. *J. Am. Chem. Soc.* **2004**, *126*, 14943.
(5) Gratzel, M., Michael *MRS Bull.* **2005**, *30*, 23.
(6) Law, M.; Greene, L. E.; Johnson, J. C.; Saykally, R.; Yang, P. D. *Nat. Mater.* **2005**, *4*, 455.
(7) Barbe, C. J.; Arendse, F.; Comte, P.; Jirousek, M.; Lenzmann, F.; Shklover, V.; Gratzel, M. *J. Am. Ceram. Soc.* **1997**, *80*, 3157.
(8) Kasuga, T. *Adv. Mater.* **1999**, *11*, 1307.
(9) Yao, B. *Appl. Phys. Lett.* **2003**, *82*, 281.
(10) Bavykin, D. V.; Parmon, V. N.; Lapkin, A. A.; Walsh, F. C. *J. Mater. Chem.* **2004**, *14*, 3370.
(11) Yuan, Z. Y.; Su, B. L. *Colloid Surf., A* **2004**, *241*, 173.
(12) Nakahira, A.; Kato, W.; Tamai, M.; Isshiki, T.; Nishio, K.; Aritani, H. *J. Mater. Sci.* **2004**, *39*, 4239.
(13) Tsai, C. C.; Teng, H. S. *Chem. Mater.* **2004**, *16*, 4352.
(14) Du, G. H.; Chen, Q.; Che, R. C.; Yuan, Z. Y.; Peng, L. M. *Appl. Phys. Lett.* **2001**, *79*, 3702.

10.1021/cm061721l CCC: $33.50 
Published on Web 11/10/2006

From these conflicting findings, different conclusions regarding the formation mechanism and crystal phase of the obtained nanostructures have been drawn. Several studies report the formation of thin nanosheet or nanoplate intermediates.[2,15,16] Two different models have been proposed to describe how these "2D precursors" are formed. In the exfoliation model, it is assumed that the basic treatment initially disturbs the crystalline structure, allowing individual 2D sheets to exfoliate from the parent crystal as complete layers (for example, (010) layers from anatase).[9] Subsequently, these sheets roll up to form scroll-like nanotubes, driven by the need to decrease surface energy or dangling bond concentration and triggered by decreasing electrostatic repulsion[8] or the formation of undercoordinated surface sites.[17] According to the dissolution/recrystallization model, the very basic environment causes partial dissolution of the $TiO_2$ and its consequent reprecipitation as layered alkali titanates. From these layered precipitates, nanotubes can be formed because of the asymmetric environment caused by hydrogen deficiency[2] or mechanical stress.[10]

Considerable efforts have been made to identify the crystal phase of the product(s), with most results indicating the formation of a protonic or alkali titanate phase. It is assumed that the sheetlike structures are formed by layers of edge-sharing $TiO_6$ octahedra; however, their precise arrangement is not clear. XRD and SAED patterns of these materials are quite complex and have been interpreted in terms of trititanate ($H_2Ti_3O_7$),[18] tetratitanate ($H_2Ti_4O_9 \cdot H_2O$),[12] pentatitanate ($H_2Ti_5O_{11} \cdot H_2O$),[11] or lepidocrocite ($H_xTi_{2-x/4}O_4 \cdot H_2O$)[16] phases. On the other hand, the exfoliation model often assumes that the nanotubes must be anatase. Recently, combined SAXS/WAXS spectra of the nanotubular material have been interpreted in terms of pseudo-anatase and pseudo-rutile phases.[17] Poudel et al. demonstrated that different crystal phases (anatase, hydrogen, or sodium titanate) are formed, depending on the autoclave filling fraction, the pH of the washing agent, and the annealing temperature.[19]

This article aims to shine some light on these contradictory findings through a systematic investigation of the relationship between preparation conditions and the size and morphology of the high aspect ratio products. It will be shown that the key element appears to be the selection of the titania precursor used, although other process parameters, such as hydrothermal temperature and solid/liquid ratio, are also important. Finally, we assess the effect of different washing procedures on the morphology of the products and their specific surface area and annealing behavior, factors that are relevant to their application in DSSCs.

(15) Chen, Q.; Zhou, W. Z.; Du, G. H.; Peng, L. M. *Adv. Mater.* **2002**, *14*, 1208.
(16) Ma, R., Renzhi *Chem. Phys. Lett.* **2003**, *380*, 577.
(17) Saponjic, Z. V.; Dimitrijevic, N. M.; Tiede, D. M.; Goshe, A. J.; Zuo, X. B.; Chen, L. X.; Barnard, A. S.; Zapol, P.; Curtiss, L.; Rajh, T. *Adv. Mater.* **2005**, *17*, 965.
(18) Chen, Q.; Du, G. H.; Zhang, S.; Peng, L. M. *Acta. Crystallogr., Sect. B* **2002**, *58*, 587.
(19) Poudel, B.; Wang, W. Z.; Dames, C.; Huang, J. Y.; Kunwar, S.; Wang, D. Z.; Banerjee, D.; Chen, G.; Ren, Z. F. *Nanotechnology* **2005**, *16*, 1935.

| Label | Crystal phase | Average particle size | Commercial source |
|---|---|---|---|
| 1 | $TiO_2$ rutile (99.5%) | several microns | Alfa Aesar |
| 2 | $TiO_2$ anatase (>99%) | ~5 nm | Nanostructured & Amorphous material |
| 3 | $TiO_2$ rutile/anatase | 30-40 nm | Nanostructured & Amorphous material |

**Figure 1.** Overview of the starting materials used.

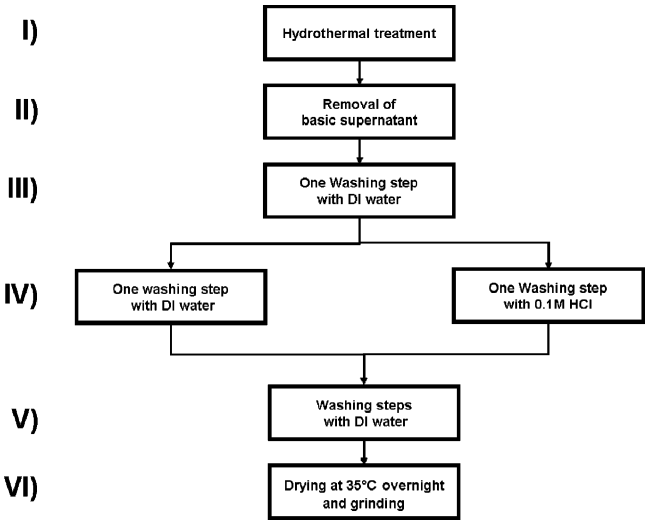


**Figure 2.** Scheme of the washing process applied after hydrothermal treatment of the titania starting powders.

## Experimental Section

Three different titania powders were used for the preparation of high aspect ratio nanostructures (see Figure 1 for details). Each of these powders was mixed with 10 M NaOH in a 250 mL Nalgene flask. The amounts of titania and basic solution were chosen to match a fixed solid/liquid ratio. The titania dispersion was heated to moderate temperatures under vigorous stirring for 2 days, after which the mixture was allowed to cool, with continued stirring, for a further 3 h.

Upon reaching room temperature, each sample was divided into 0.25 g batches and treated as illustrated in Figure 2. Each washing step consisted of mixing the precipitate of the previous step with 35 mL of the washing agent, sonicating for 15 min, and finally centrifuging in order to isolate the solid product. Stages II and III of the washing procedure (shown in Figure 2) were intended to remove the majority of the highly basic hydrothermal solution. At stage IV, with the solution still very alkaline, some variation was introduced into the washing procedure: the sample was mixed with either 35 mL of deionized (DI) water as in the previous steps, or an equivalent amount of 0.1 M HCl; the resulting final products are referred to as water-washed and acid-washed samples, respectively. As a further variation, the washing agent was added in one of two modes: either in a single addition or dropwise over a 2 h period with stirring. In stage V, further washing steps with DI water followed (8 washing steps by single addition of DI water, unless otherwise stated). After the final washing step, the wet material was dried in air at 35 °C and finely ground in a mortar. Selected samples (~0.1 g) were annealed in a furnace under air at 450 °C for 2 h.

SEM images and EDX data were collected on a GEMINI LEO 1525 FEGSEM and a Philips XL-30 FESEM at an accelerating voltage of 5 kV. Samples for characterization were sonicated in ethanol, deposited on a fluorine-doped tin oxide (FTO) substrate,

and coated with 15 nm of gold. TEM images and SAED patterns were obtained on a JEOL 2000FX, operating at 200 kV; samples were sonicated in ethanol or water and deposited onto a holey carbon film. XRD measurements were performed on a Philips PW1729 X-ray diffractometer using Cu−Kα radiation. Raman spectra of the powders were collected on a LabRam Infinity Raman spectrometer, using 532 and 633 nm lasers. The determination of specific surface areas were determined by BET adsorption measurements on a Micromeritics ASAP 2010 instrument.

## Results and Discussion

**Influence of the Starting Materials.** Titania powders of different crystal phases and average particle sizes were transformed into high aspect ratio (HAR) nanostructures by applying a standard set of hydrothermal and washing conditions (solid/liquid ratio: 1 g of $TiO_2$/60 mL of 10 M NaOH solution; 130 °C hydrothermal temperature; 8 DI water-washing steps, single addition of the washing agent).

As shown in Figure 3, SEM shows that the products have different structures depending on the starting powder used. Products from powders **1** and **2** are similar in morphology and size (see images a and b of Figure 3), even though the particle size of the precursor powders differs by more than 3 orders of magnitude (see Figure 1). The products obtained from these two powders have a rodlike morphology, with no obvious hollow core, and exhibit a broad distribution of diameters and lengths (average values: $d \approx (50 \pm 30)$ nm and $l \approx (2 \pm 2)$ $\mu$m). The apparent slight difference in length between these two samples is probably an artifact of sample preparation; samples taken directly from the hydrothermal mixture show much longer (several tens of micrometers) fiberlike structures (see Figure 9), which must break during subsequent sonication and grinding steps. However, the general similarity of morphology and diameters of both products clearly demonstrates that the dimensions of the products are not directly correlated to those of the starting materials. This conclusion provides a strong argument against the exfoliation mechanism, and in favor of the dissolution/recrystallization model. On the other hand, the X-ray data and Raman spectra of products obtained under identical experimental conditions but at a slightly lower temperature of 110 °C (not shown) indicate that the products obtained from microcrystalline powder **1** contain original starting material, whereas the products from nanocrystalline powder **2** are fully converted. This impact of the crystal size on the conversion yield, which is in agreement with the findings of Nakahira et al.,[12] may be attributed to the higher surface area and lower stability of the nanoscale precursor. These conclusions may explain the findings of Zhang et al.,[20] who claimed that both the crystal phase and the size of the precursor influence nanotube formation; their observation of different $N_2$ adsorption behavior for different initial particle sizes can probably be attributed to variations in conversion yield rather than variations in the high aspect ratio morphologies. Although particle size is the most obvious difference between powders **1** and **2**, the identity of the crystal phases may also have an effect.

(20) Zhang, Q. H.; Gao, L. A.; Sun, J.; Zheng, S. *Chem. Lett.* **2002**, 226.

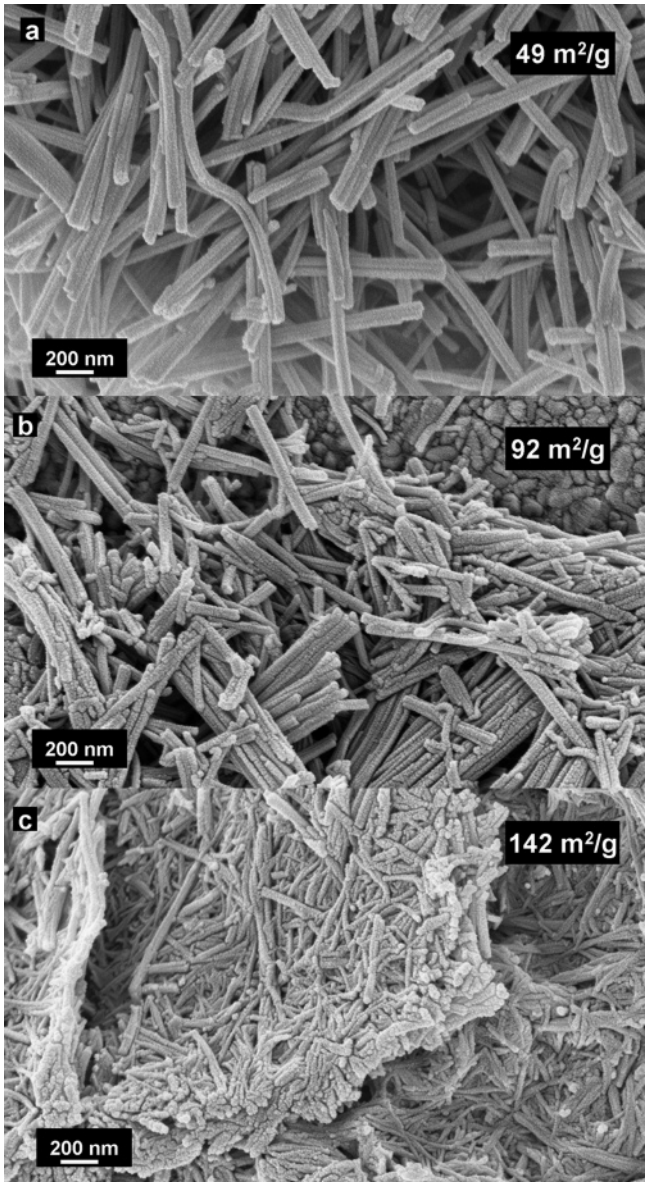


**Figure 3.** SEM images and specific (BET) surface areas (inset) of HAR structures obtained after hydrothermal treatment of different starting materials: (a) product from microcrystalline $TiO_2$ rutile powder **1**, (b) product from nanocrystalline $TiO_2$ anatase powder **2** (note that the granular structure in the background originates from the substrate), and (c) product from nanocrystalline $TiO_2$ rutile/anatase powder **3**. Experimental details: solid to liquid ratio, 1 g of $TiO_2$/60 mL of 10 M NaOH solution; hydrothermal treatment at 130 °C for 2 days; 8 washing steps with DI water; single addition of washing agents.

Returning to Figure 3, the products from powder **3** are distinctly different from those of powders **1** and **2**; both SEM and TEM images (see Figures 3c and 4d) show that smaller and more uniform products are obtained when the mixed-phase precursors are used. The TEM images (Figure 4d) show a high fraction of hollow structures with diameters around 10−15 nm and several hundreds of nanometers in length. These values are consistent with those frequently reported for titania nanotubes.[2,9,10] In addition, the surface area is significantly greater (142 $m^2/g$) than for both the larger structures, as might be expected. In fact, this surface area is broadly consistent with a simple geometric estimate for tubes of these dimensions (assuming perfect tubes with ID 5 nm and OD 12.5 nm and using the $Na_2Ti_3O_7$ bulk density of 3.94 $g/m^3$, we can perform a simple geometric calculation

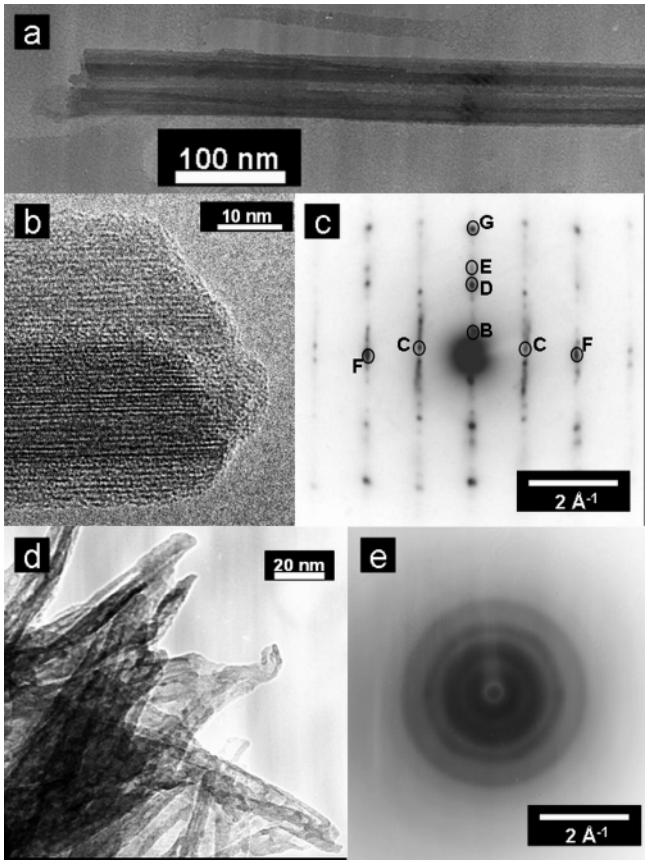


**Figure 4.** TEM images of HAR structures obtained from (a) microcrystalline rutile powder **1**, (b) nanocrystalline anatase powder **2**, and (d) nanocrystalline $TiO_2$ rutile/anatase powder **3**. (c) and (e) show indicative SAED patterns for structures (a) and (d), respectively. Experimental details as for Figure 3.

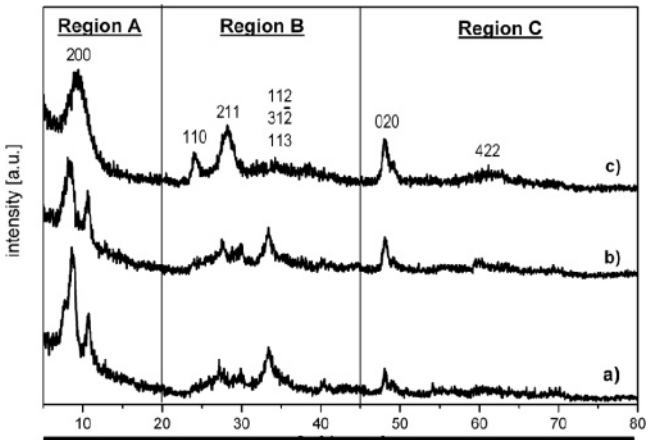


| Products from $TiO_2$ powder 1 | | | |
|---|---|---|---|
| label | d-spacing from XRD (Å) | d-spacing from SAED (Å) | index acc. to pentatitanate model |
| A | 10.3 | | 200 |
| B | 8.3 | 8.0 | 20$\bar{2}$ |
| C | 3.7 | 3.7 | 110 |
| D | 2.7 | 2.8 | 005 |
| E | 2.2 | 2.3 | 006 |
| F | 1.9 | 1.9 | 020 |
| G | 1.5 | 1.6 | 10 0 3 |

**Figure 5.** X-ray diffraction patterns of HAR structures obtained from different starting materials: (a) products from $TiO_2$ rutile powder **1**, (b) products from $TiO_2$ anatase powder **2**, and (c) products from $TiO_2$ rutile/anatase powder **3** (indexed as trititanate $H_2Ti_3O_7$ according to Chen et al.[18]). The table compares the *d*-spacings obtained from pattern (a) with the *d*-spacings obtained from the SAED pattern shown in Figure 4c (bold numbers indicate strong signals) and indexes the reflections according to the model of hydrated pentatitanate $H_2Ti_5O_{11}{\cdot}3H_2O$.[22] Experimental details as for Figure 3.

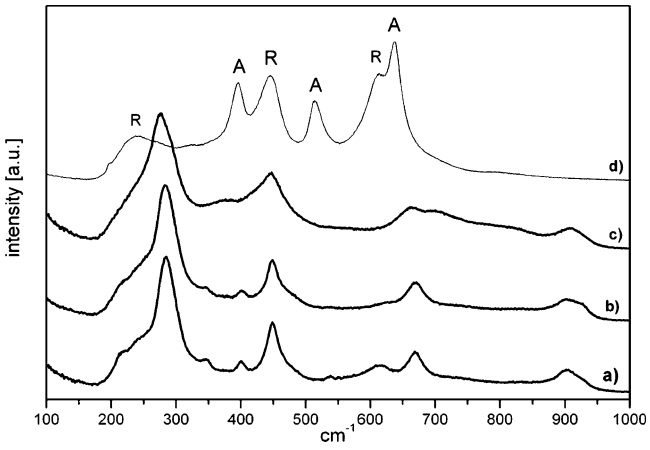


**Figure 6.** Raman spectra ($\lambda_{ex} = 633$ nm) of HAR structures obtained from different $TiO_2$ starting materials: (a) products from rutile powder **1**, (b) products from anatase powder **2**, and (c) products from rutile/anatase powder **3**. For reference, line (d) shows the spectrum of the initial powder **3** with the anatase and rutile peaks marked as A and R, respectively. Experimental details as for Figure 3.

that yields a surface area of 135 $m^2/g$). The SAED pattern of powder **3** (see Figure 4e) shows distinct but quite broad rings, indicating crystallinity but small crystal sizes or high defect concentrations (note that the SAED pattern originates from several nanostructures, giving rise to orientational averaging).

TEM images of the products from powders **1** and **2** (see images a and b of Figure 4) show only larger high aspect ratio structures, often termed nanofibers, nanobelts, or nanoribbons.[11,21] Within each individual nanofiber, the internal contrast is consistent with a uniform cross-section along the nanofiber axis. The presence of these smaller substructures suggests that the nanofibers consist of irregularly folded layers, rather than uniformly (sc)rolled tubes, which leads to complex internal structures, as seen for the individual nanofibe shown in Figure 4a. The surface areas for these nanofibers are bigger than might be expected given their external geometry. Assuming perfect cylinders with a diameter of 50 nm and using the $Na_2Ti_3O_7$ bulk density of 3.94 $g/m^3$, we can perform a simple geometric calculation that yields a surface area of 20 $m^2/g$ compared to values of 49 and 92 $m^2/g$ measured by the BET method. This discrepancy suggests substantial $N_2$ adsorption, either in interlayer galleries or in internal cavities generated by the irregular folding. The SAED patterns of the individual nanostructures obtained from powders **1** and **2** are similar; a typical example is shown in Figure 4c. All the diffraction patterns from the nanofibers have a similar appearance, with the same crystallographic orientation; however, variations in the equatorial spacings occur. The spacings observed in the diffraction pattern of the nanotubular products (Figure 4e) compare reasonably well to those of the nanofibrous products (Figure 4c), considering the rotational averaging

(21) Yang, H. G.; Zeng, H. C. *J. Am. Chem. Soc.* **2005**, *127*, 270.

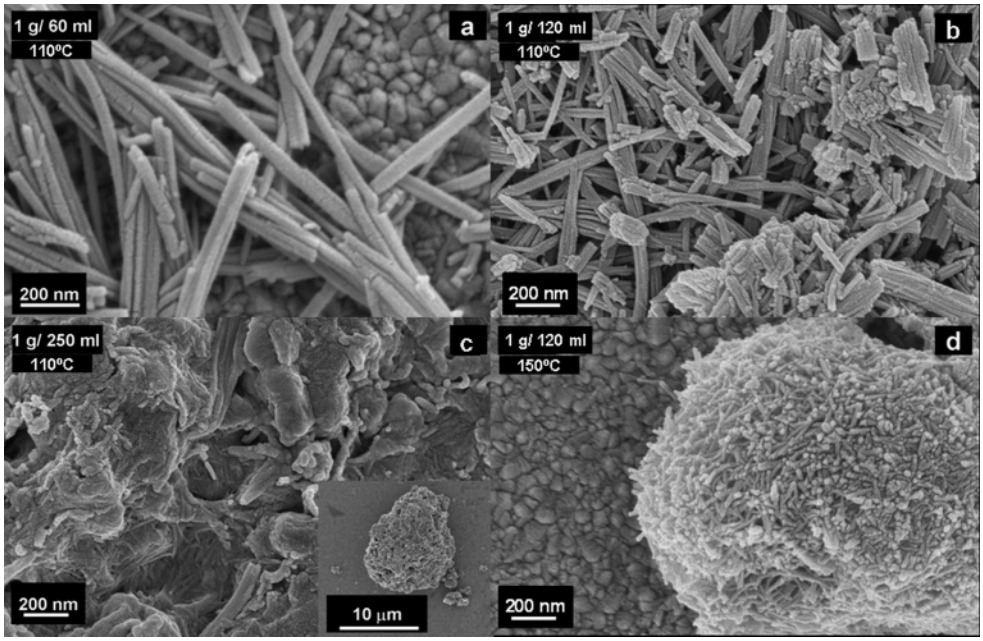


**Figure 7.** SEM micrographs of materials obtained from microcrystalline $TiO_2$ rutile powder **1** at different temperatures and solid/liquid ratios ($TiO_2$/NaOH solution): (a) 110 °C, 1 g/60 mL; (b) 110 °C, 1 g/120 mL; (c) 110 °C, 1 g/250 mL (inset shows the same particle at lower magnification); and (d) 150 °C, 1 g/120 mL. See Figure 3 for additional experimental details. Note that the granular structure observed in the background originates from the substrate.

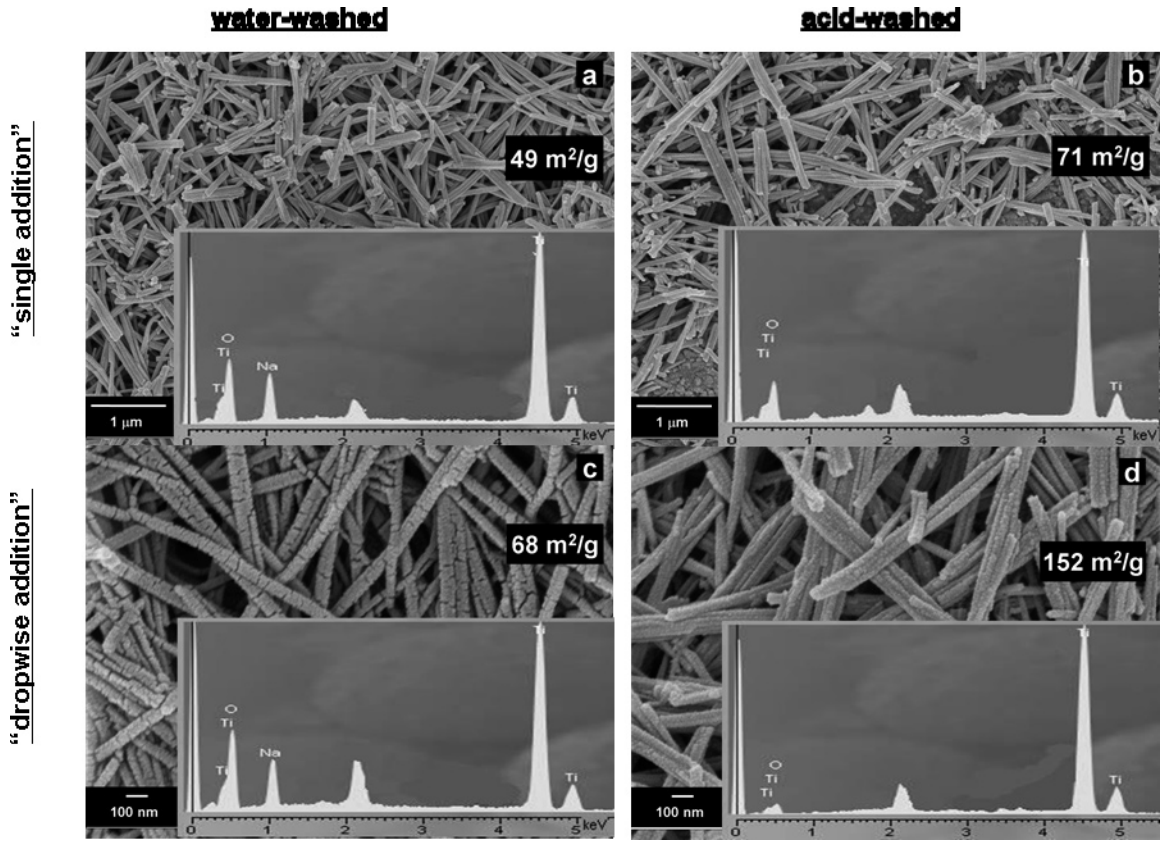


**Figure 8.** SEM images, specific surface areas, and EDX spectra of products from microcrystalline $TiO_2$ rutile powder **1**: (a,c) after water-washing and (b,d) after acid-washing with 0.1 M HCl (see step IV in Figure 2). Washing agents were introduced either in (a,b) single addition or (c,d) dropwise. See Figure 3 for additional experimental details.

involved; however, given the breadth of the nanotube peaks, X-ray data provide a more useful comparison.

The X-ray diffraction patterns of the products are shown in Figure 5. The data for the products from precursor **3** (Figure 5c) resemble those reported in the literature for titanate nanotubes, and reflections can be indexed as either trititanate[18] or tetratitanate[12] phases. In contrast, X-ray patterns of the products from precursors **1** and **2** (panels a and b of Figure 5, respectively), although similar to each other, have a distinctly different appearance. Some features are less well defined and the assignment of the peak reflections is not straightforward, as few comparable spectra

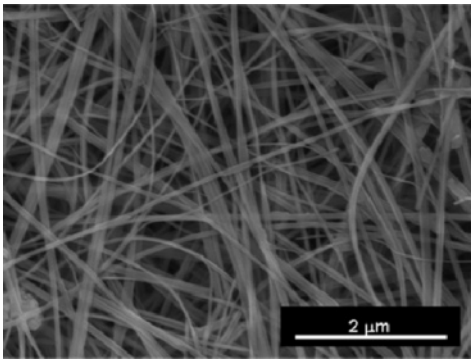


**Figure 9.** SEM image of product from microcrystalline $TiO_2$ rutile powder **1** before washing. See Figure 3a for other experimental details.

are available in the literature that relate to $TiO_2$, titanates, or HAR $TiO_x$ nanostructures. Peak positions most closely resemble those reported for hydrated pentatitanate ($H_2Ti_5O_{11}\cdot H_2O$).[22]

For a more detailed analysis, the XRD spectra can be divided into three regions (see Figure 5). The three products show similar reflections for small *d*-spacings (region C). In particular, there is a common signal at $d = 1.86$ Å ($2\theta = 48.04°$), which can be found in different bulk titanates and is probably linked to the Ti separation in layers of the edge-shared $TiO_6$ octahedra.[23] The spectra show clearer discrepancies in regions A and B. In region B, the patterns indicate differences in the $TiO_6$ framework, most likely due to a difference in the step length of the titanate sheets; the range of indistinct peaks in panels a and b of Figure 5, around 25−30°, suggests a degree of irregularity in these materials. The products also differ in region A ($d > 4$ Å), which relates to interlayer spacings. In general, the presence of signals in this region proves that all products have a layered titanate framework.[22,24,25] Again, products from powders **1** and **2** are similar, with two major peaks in this region, which may correspond to sodium ion or proton intercalated layers or to variations in water content. Sasaki et al. demonstrated that pentatitanate species with different interlayer distances ($x$) can coexist during ion exchange experiments; namely, $H_2Ti_5O_{11}\cdot 3H_2O$ ($x = 10.4$ Å) and $KHTi_5O_{11}\cdot nH_2O$ ($x = 8.8$ Å).[22] In the case of the products from powder **3**, these peaks are broadened to a single feature, almost certainly due to the small size and high radius of curvature of the titanate layers. A calculation of the crystal domain size using the Scherrer equation on the basis of the width of the interlayer XRD peak (region A) gives a value of 8 nm for products from powders **1** and **2** and 2 nm for products from powder **3**. These values, which indicate the crystallite size perpendicular to the tube/fiber axis, are consistent with the differences in morphology and crystal domain size observed by electron microscopy.

As summarized in Figure 5, the results obtained by SAED for the products of $TiO_2$ rutile powder **1** (see Figure 4c) are in good agreement with the XRD results. The spacings in regions B and C are very similar for both diffraction methods, although minor variations in region B may arise when studying an individual nanofiber rather than an average of structures containing different titanates. In region A, the agreement between the methods is poorer, probably because of dehydration effects in the vacuum of the electron microscope; in any case, the equatorial features in the SAED patterns corresponding to the layer spacings vary between individual structures. However, the orientation of the titanate lattice is constant among all of the nanofiber products. The spacing of 1.9 Å always appears on the meridian of the SAED pattern (F in Figure 4c, corresponding to reflection (020) in pentatitanate). Regardless of the specific titanate, this spacing is characteristic of the point-to-point distance of the titania octahedra, which correspondingly must be aligned parallel to the nanofiber axis. Conversely, a spacing around 2.8 Å always appears on the equator (D in Figure 4c, corresponding to reflection (005) in pentatitanate), which is characteristic of the approximate width of a titania octahedron. Other spacings on the equator (B, E, G in Figure 4c) are more variable between nanofibers depending on the titanate, but share a zone axis (pentatitanate (020) for the example given). The appearance of the diffraction pattern is indeed characteristic of the cylindrical rotational averaging associated with fibers (and nanotubes). Thus, it is clear that the nanofibers are all based on curved titanate sheets of edge-sharing octahedra that point along the fiber axis. This suggestion is a generalization of the trititanate model of Chen et al.[18] This characteristic structure can perhaps be attributed to the different flexibility of the sheet in the two orthogonal directions: the step edges in titanate structures provide vertex-linked bands, which may allow folding or scrolling in one direction, whereas consistent edge sharing prevents curvature parallel to the axis.

The Raman spectra of the products are shown in Figure 6, with the anatase/rutile starting material used as a reference. In general, the spectra obtained from different titania sources are similar, although, again, the products from powders **1** and **2** match closely, whereas the product from powder **3** is slightly different and exhibits broader peaks. The absence of a set of bands corresponding to conventional titania phases, such as anatase or rutile, clearly indicates the rearrangement of the nanostructured materials into new crystal phases. Only the shoulder at 250 $cm^{-1}$ and the peak at 447 $cm^{-1}$ can be allocated to modes of $TiO_2$ rutile.[26] These signals are present in all three spectra and probably indicate a common $TiO_6$ building block, similarly to the reflection at $2\theta = 48°$ ($d = 1.89$ Å) in the XRD pattern. The peak at ~670 $cm^{-1}$ is probably intrinsic to these nanostructured products, but may relate to the $B_{1g}$ anatase mode, which has been assigned to the Ti−O stretching vibration in edge-shared $TiO_6$,[23] and which can shift because of oxygen deficiency or bending of the structure.[27] Similarly, the presence of edge-linked octahedral may explain the feature at 401 $cm^{-1}$, which also occurs in anatase. On the other hand, the absence of pronounced bands around 750 $cm^{-1}$ indicates the absence of corner-shared $TiO_6$ units.[23] The peaks at 285

(22) Sasaki, T., Takayoshi *Chem. Mater.* **1992**, *4*, 894.
(23) Su, Y.; Yali *J. Phys. Chem. B* **2000**, *104*, 8160.
(24) Feist, T., Thomas *J. Solid State Chem.* **1992**, *101*, 275.
(25) Suzuki, Y.; Yoshikawa, S. *J. Mater. Res.* **2004**, *19*, 982.
(26) Qian, L.; Du, Z. L.; Yang, S. Y.; Jin, Z. S. *J. Mol. Struct.* **2005**, *749*, 103.
(27) Parker, J. *Appl. Phys. Lett.* **1990**, *57*, 943.

$cm^{-1}$ and ~900 $cm^{-1}$ are intrinsic to the new titanate phases. The former peak is hard to assign, but has been reported to be due to vibrations between sodium and oxygen bonds.[23] Our experiments, as well as findings by Papp et al.,[28] suggest that this allocation to the presence of sodium is questionable, as the Raman spectra of products after water-washing (leaving sodium in the structure) and acid-washing (removing sodium from the structure) both show strong bands around 280 $cm^{-1}$ (see Figure 6 and the Supporting Information, Figure S1, respectively; further information about the effect of washing is given below). The band at ~285 $cm^{-1}$ may, therefore, rather relate to a break of symmetry in the rearranged and bent $TiO_6$ layers. The band at ~900 $cm^{-1}$ can be related to a short symmetric Ti−O stretching mode, characteristic of short Ti−$O^-$ bonds.[23,29] A more general comparison with Raman data for bulk alkaline titanates shows that the spectra of the as-prepared HAR structures exhibit less-distinct signals and have much broader bands. This trend can be attributed either to lower crystallinity in the nanoscaled products and variability in the specific titanate phase present, or to the variable curvature of the edge-sharing layers. This broadening may result in the loss of further Raman peaks that are usually observed in the spectra of bulk titanates; however, the nanostructured materials do not show any additional bands that cannot be found in conventional bulk titanates.

To summarize this section, it is clear that the starting material can have a dramatic impact on the morphology, size, and detailed crystal structure of the high aspect ratio products. This conclusion is in agreement with some papers but not others.[11,12,14,20] The apparent contradiction may arise from the complexity of the reaction. Thus, both microcrystalline rutile and nanocrystalline anatase give similar nanostructured products, despite the dramatic difference in starting material. There are indications that the particle size simply influences the conversion yield,[12] a factor that can easily be overlooked. The phase-pure starting materials seem to favor the formation of compact, single-crystalline nanostructures with fibrous or rodlike morphology, consisting of axially folded titanate layers. On the other hand, the mixture of rutile and anatase crystal phases seems to be best suited to form titanate nanotubes; indeed, other groups have reported using similar mixed-phase[13,26] or amorphous[30] $TiO_2$ starting materials. A possible explanation is that the mixed-phase or amorphous material contains a high concentration of defects, destabilizing the starting materials and accelerating the initial dissolution; subsequent recrystallization can then occur from a concentrated precursor solution, leading to rapid nucleation of small HAR nanostructures.

**Influence of Other Hydrothermal Parameters.** In order to explore discrepancies in the literature further, we investigated other parameters, namely hydrothermal temperature, solid/liquid ratio, and washing procedure. These experiments were performed using the microcrystalline $TiO_2$ rutile powder **1** as starting material.

It is obvious from Figure 7 that both the temperature of the hydrothermal process and the solid/liquid ratio influence the size and morphology of the final nanostructures. At a high liquid content (excess base), large equiaxed particles, up to 10 $\mu$m in diameter, appear instead of high aspect ratio structures (Figure 7b). At high fractions of concentrated base, the initial titania powder is likely to dissolve completely, without precipitating into layered titanate nanosheets under hydrothermal conditions; subsequent washing precipitates the formless product (see further discussion on washing below). At a solid/liquid ratio of 1 g of $TiO_2$/120 mL of NaOH solution, the higher temperature of 150 °C (Figure 7d) produces dense aggregates of smaller structures that have dimensions frequently reported for titanate nanotubes and similar to those seen in Figure 4d). However, it should be noted that the latter experiment was not conducted in a Nalgene flask (because the higher temperature) but in an autoclave without stirring. Taking also Proudel's findings about the role of the autoclave filling fraction and pressure into account,[19] it is hard to decide if this change in morphology is an exclusive temperature effect. However, the essential influence of these parameters demonstrates the importance of optimizing the preparation conditions for a given starting material. Of course, the delicate equilibrium between the dissolution of the titania and the precipitation of the titanate nanostructures also provides great flexibility to a relatively cheap and simple process.

**Influence of the Washing Procedure on Nanostructure Formation.** Finally, using the microcrystalline $TiO_2$ rutile powder **1** and the conditions described above to obtain compact rodlike structures (110 °C hydrothermal temperature, solid/liquid ratio of 1 g/60 mL), the influence of the final washing procedure (see Figure 2, step IV) was explored. It has often been suggested that the rolling of sheetlike precursors occurs during the washing process.[8,13] In order to explore whether the washing procedure has any impact on final morphology, different neutralization approaches (acid- or water-washing), different numbers of DI water-washing steps (7 or 15), and different methods of addition of the washing agent (single addition or dropwise) were investigated.

Minimal differences in morphology were revealed in any of these cases using X-ray diffraction (see the Supporting Information, Figure S2) or SEM (see Figure 8). Contradictory findings have been reported previously but relate to different starting materials and, in particular, to the formation of nanotubes rather than nanofibers.[8,13] To explore the effect of the washing procedure further, samples were taken directly from the hydrothermal mixture, without being subjected to any washing step (after step II in Figure 2). Figure 9a shows a SEM image of the corresponding samples, revealing that a network of nanofibrous structures tens of micrometers long already exists in the hydrothermal mixture prior to washing.

This observation implies that the morphology and dimensions of the nanostructures are determined by the hydrothermal treatment, rather than by the washing process. The results in this study are consistent with a dissolution and recrystallization mechanism, as proposed by Kukovescz et

(28) Papp, S.; Szilvia *J. Solid State Chem.* **2005**, *178*, 1614.
(29) Byeon, S. *J. Solid State Chem.* **1997**, *130*, 110.
(30) Wu, D.; Liu, J.; Zhao, X. N.; Li, A. D.; Chen, Y. F.; Ming, N. B. *Chem. Mater.* **2006**, *18*, 547.

al.,[31] in which oriented crystal growth takes place from nanometer-sized seeds. According to this mechanism, the presence of small curved objects, so-called "nanoloops", in the very early phases of the hydrothermal treatment determines the morphology of the final product. In our study, the observed insensitivity of the products toward the washing procedure, together with a clear dependence on the hydrothermal conditions, strongly support a growth process rather than a pH- or charge-driven rolling.

**Other Effects of the Washing Procedure.** Despite not having an effect on the product morphology, the acidity of the washing agent did have significant influence on other important properties of the final nanostructures, namely specific surface area, elemental composition, and annealing behavior. These properties are crucial for potential applications of these HAR materials. For instance, high surface areas are desirable for catalytic applications,[13] as well as for DSSC electrodes.[4] The annealing behavior is also an important factor in the fabrication of DSSCs,[7] where there is an interest in converting the titanate nanostructures into highly crystalline anatase while retaining their high aspect ratio.

Figure 8 illustrates the effect of water-washing (images a and c of Figure 8) and acid-washing (images b and d of Figure 8) on the final morphology of titanate nanofibers. Whereas water-washed samples remained basic (pH ~9), acid-washed samples reached the pH of the DI water (pH 6). Complete neutralization of the basic samples was not achieved through water-washing only, even after 15 washing steps. Neutral samples appeared to disperse more readily than the basic ones, which is an important benefit for many applications, including the fabrication of uniform, mesoporous DSSC electrodes.[7] Moreover, the acid treatments significantly increased the specific surface area of the products (e.g., 152 $m^2/g$ for the sample in Figure 8d compared to 68 $m^2/g$ for that in Figure 8c). This difference in surface area is surprising, given the apparently unaltered morphology of the products (as judged by electron microscopy), but can be attributed to intercalation chemistry. As noted above, the relatively high absolute value of the surface area implies that internal surfaces of the nanofibers must play an important role in all cases. EDX data (see insets in Figure 8) shows that the material formed during hydrothermal treatment contains sodium ions, which are almost certainly accommodated between the octahedral titania layers, following the classic sodium titanate structure.[24] A (semi)-quantative analysis of the EDX data provides an estimate for the Na/Ti molar ratio of around 0.5; the figure is broadly consistent with titanate compositions and indicates that the water-washing does not remove the intercalated sodium. Upon treatment with diluted acid, the majority of these ions are removed (the Na/Ti ratio drops to 0−0.1) and replaced with protons and/or water molecules.[28] The removal of the larger sodium ions apparently makes the interlayer space more accessible to $N_2$ molecules during the BET measurement, resulting in higher specific surface areas without altering the external morphology. Broadly, similar effects are observed for the nanotubular structures synthesized from anatase/rutile powder **3** (as in Figure 3c), with the surface area increasing from 142 to 282 $m^2/g$ for single addition-water-washed and single addition acid-washed samples, respectively. The higher absolute surface area is consistent with the smaller size and greater accessibility of the nanotubular structures.

It is interesting to note from Figure 8 that dropwise addition of washing agent increases the surface area dramatically, compared to a rapid single addition. The effect is significant for water-washed samples (images a and c of Figure 8), but is more pronounced for acid-washed samples (images b and d of Figure 8), with surface area increasing from 71 to 152 $m^2/g$. This observation is consistent with the more effective deintercalation of sodium using dropwise addition of acid. The slow addition of acid presumably provides the greatest scope for equilibration throughout the structure, maximizing the ion exchange and the opening of the interlayer galleries in the structures.

Last, the annealing behavior of the nanofibrous and nanotubular products obtained from powders **1** and **3**, respectively, was compared. Figure 10 shows SEM images of products obtained after annealing for 2 h at 450 °C and their corresponding Raman spectra before and after heat treatment. Under the conditions studied, only HCl-treated samples transformed into anatase (see images b and d of Figure 10). Apparently, the sodium ions retained in the water-washed material stabilize the titanate structure. After acid-washing, the sodium ions are replaced by protons (and water), which in turn can be removed relatively easily by dehydration. This conclusion is consistent with work on bulk trititanates by Papp et al.[28] The overall morphology after annealing also depends on the sodium content; unsurprisingly, the water-washed samples, which do not convert to anatase, mostly retain their high aspect ratio structure, although some polycrystalline granular material does appear (see images a and c of Figure 10). In contrast, the response of the acid-washed samples, which convert to anatase, depends on the morphology of the titanate nanostructures. The conversion of nanotubes (from powder **3**) is linked to a dramatic loss of aspect ratio (see Figure 10d), suggesting that a tubular form is, in fact, not favorable for anatase. On the other hand, the nanofibrous structures (from powder **1**) retain their high aspect ratio (see Figure 10b); apparently, the fibers are sufficiently large and dense to convert into polycrystalline anatase without critical weakening.

## Conclusion

This paper explores the hydrothermal synthesis of high aspect ratio titania nanostructures, identifying two categories of products: nanofibers and nanotubes. The nature of the product critically depends on the nature of the starting material, with mixed anatase/rutile starting powder proving to be preferable for nanotube synthesis. On the other hand, we have found that the dimensions of the final particles are not controlled by those of the starting material. This fact, together with the insensitivity of the product morphology to the washing conditions and the identification of high aspect ratio structures prior to the washing procedure, support a

(31) Kukovecz, A.; Hodos, N.; Horvath, E.; Radnoczi, G.; Konya, Z.; Kiricsi, I. *J. Phys. Chem. B* **2005**, *109*, 17781.

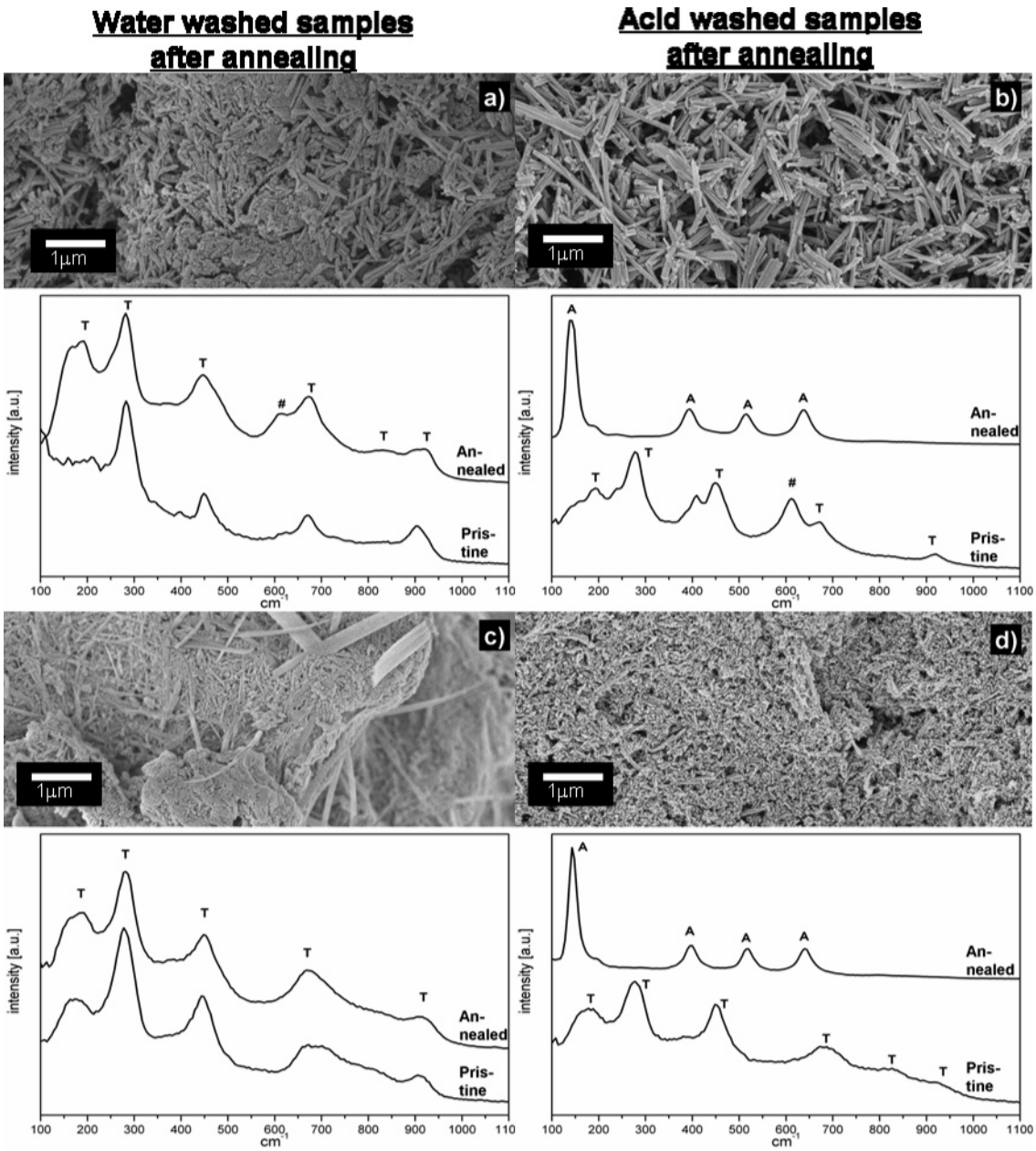


**Figure 10.** SEM micrographs of (a,b) annealed nanofiber products from powder **1** and (c,d) annealed nanotubular products from powder **3**. Samples were subjected to different washing treatments: (a,c) water-washed and (b,d) acid-washed. Insets show Raman spectra ($\lambda_{ex} = 532$ nm) of pristine and annealed materials (where *T* denotes titanate signals, *A* denotes anatase signals, and # indicates signals from the $TiO_2$ starting powder). Note the somewhat-altered appearance of the Raman spectra of the pristine products compared to Figure 6, due to the use of a different laser wavelength. Experimental conditions as for Figure 3; single addition of washing agents; annealing for 2 h at 450 °C.

dissolution/recrystallization[25] mechanism during hydrothermal treatment, rather than an exfoliation or rolling mechanism. Raman, XRD, and SAED data all confirm that all products are based on layered titanates, with some variation in specific type both between nanotubes and nanofibers and within individual samples. Indeed the existence of curved and tubular forms of titanate layers is quite consistent with the general understanding of nanotube energetics; the occurrence of true anatase nanotubes would be much more surprising given the more modest degree of anisotropy in the underlying crystal structure.

Changing the ratio of base to starting material was found to have an important influence on the reaction products, with excess base suppressing nanoparticle reprecipitation. Many of the conflicting findings and interpretations in the current literature could be attributed to variations in the initial starting materials and in the starting material/base ratio, which is often not reported.

Although the washing procedure did not affect the overall morphology of the final products, the use of an acid wash was found to remove sodium ions from the structure, thus increasing the surface area in the galleries of the layered structure and enabling its thermal conversion to anatase. For applications, high surface area, high aspect ratio anatase particles are probably of most interest. This paper describes how to synthesize nanofibrous structures of such materials. Small titanate nanotubes have higher surface area than nanofibers; however, in our studies, they do not appear to be stable on thermal conversion to anatase. Further investigation is required. Our findings clearly demonstrate the

sensitivity of the reaction to the experimental conditions, but also the flexibility and potentiality of the method.

**Acknowledgment.** R.M. acknowledges the Engineering and Physical Sciences Research Council for funding. A.M.P. acknowledges the Spanish Secretaría de Estado de Universidades e Investigación del Ministerio de Educación y Ciencia for a postdoctoral fellowship.

**Supporting Information Available:** Raman spectra of acid-washed HAR products obtained from powder 1, 2, and 3 and X-ray diffraction patterns of products from powder 1 after different washing procedures (PDF). This material is available free of charge via the Internet at http://pubs.acs.org.

CM061721L